Research Square

Preprints are preliminary reports that have not undergone peer review.
They should not be considered conclusive, used to inform clinical practice,
or referenced by the media as validated information.

A traceable framework for comparing historic pagoda morphology from 3D heritage meshes

JunLei Zhu
YiFeng Fan
20000297@dlnu.edu.cn

Article

Keywords:

Posted Date: November 12th, 2026

DOI: https://doi.org/10.21203/rs.3.rs-11369921/v1

License: This work is licensed under a Creative Commons Attribution 4.0 International License.
Read Full License

Additional Declarations: No competing interests reported.

A traceable framework for comparing historic pagoda morphology from 3D heritage meshes

JunLei Zhu[1], YiFeng Fan[1]*

[1] School of Design, Dalian Minzu University, Dalian 116600, China

*Corresponding author: YiFeng Fan

Email: 20000297@dlnu.edu.cn

Abstract

The arrangement of successive roofs gives historic pagodas different patterns of narrowing that overall proportions alone do not fully describe. Chaoyang North and Chongshou Temple have similar last-to-first studied eave-width ratios, yet at one-quarter of the height between these eaves they retain 76% and 90% of their respective first-eave widths. Their difference is concentrated in the lower roof sequence. We compare eave-width profiles from 3D heritage meshes, retaining each eave's relative height and checking the measured boundaries. Four pagodas support the main comparison; Liaoyang is examined separately where boundaries remain unresolved. Qingzhou White combines less initial narrowing with greater relative eave spacing than Chongxing Temple West. Both quarter-height contrasts persist under tested measurement choices, although profile distances vary. These comparisons identify roof intervals for subsequent surveys of wall positions, bracket reach and roof projections.

Introduction

A historic pagoda's outline combines the narrowing of successive roofs with the spaces between them. Two sequences can end at similar proportions while concentrating their changes in different parts of the building. Locating those differences turns a comparison of silhouettes into a question about particular roof assemblies and their supporting components. Eaves, the projecting roof edges, provide repeated architectural boundaries through which to examine this question.

Existing studies connect pagoda form to dimensions and components. Wang et al. examine geometric patterns and dimensional modules in Tang brick pagodas[1], while Qiu and Cheng investigate pavilion-style forms through parametric geometry[2]. Gao et al. classify Liao tower-body wall compositions through openings and sculpture[3]. These studies address different aspects of architectural organization. We build on them by examining where width reduction occurs along recorded roof sequences, identifying roof intervals in which an apparent similarity in overall taper breaks down.

Photogrammetry and 3D scanning provide digital records from which architectural measurements can be extracted[4]. Pagoda-specific methods estimate central axes and quantify rotational and reflectional symmetry[5,6]. These methods organize recorded geometry, but do not by themselves establish the architectural identity of a particular extremum. The farthest point may lie on a bell, branch, ornament or reconstruction artefact. An incomplete surface can interrupt an otherwise recognizable eave, while sampling density and reconstruction deformation also affect the geometry[7,8]. Measuring an eave therefore requires checking whether both endpoints belong to its intended continuous boundary.

Semantic segmentation assigns architectural labels to point clouds[9], provenance models connect geometry with interpretation[10], and mesh-defect documentation records local expert judgments[11]. Specifications and processing metadata further support reuse[12,13]. These contributions raise a specific question for morphological comparison:

does an uncertain edge change the inferred location of narrowing, or only the support for describing a particular roof? Connecting boundary identification to the profile allows both consequences to be examined.

We ask whether similar reductions between the lowest and highest studied eaves conceal different distributions of narrowing, and which contrasts persist when measurement choices change or an uncertain eave is omitted. Each measured width retains its relative height between the first and last studied eaves. This represents the selected roof sequence, rather than the whole tower, and permits comparison of different eave counts without equating equally numbered tiers.

Chaoyang North and Chongshou Temple, each represented by thirteen eaves, test what similar overall reductions conceal. Qingzhou White and Chongxing Temple West, with seven and thirteen, examine narrowing alongside relative roof spacing. Boundary review and sensitivity tests support these comparisons; Liaoyang White provides a separate conditional analysis of unresolved evidence. The framework links findings to measured edges and comparison choices (Figs. 1 and 2), locating roofs for component investigation. These selected cases do not isolate causes of differences between architectural types.

Methods

Study objects and eave boundaries

We examined Chaoyang North (CY), Chongshou Temple (CS), Qingzhou White (QZ), Chongxing Temple West (CX) and Liaoyang White (LY) Pagodas. QZ has seven studied eaves; the others have 13, numbered upward. The study range extends from the first to the last selected eave. Four cases support the main comparison. LY is included in a separate conditional analysis to illustrate comparisons with unresolved boundary evidence (Table 1). Its results therefore do not have the same evidential status as those of the four main cases. The curve used in this analysis is termed the conditional profile.

CY has a square plan; the other cases are octagonal. Original aerial images and ContextCapture projects are available for LY and CX. The other three supplied models have incomplete acquisition histories. The two case pairs were chosen to interpret differences in the available profiles. They were not sampled to test differences between architectural types.

Table 1 Pagodas and the eave sequences included in the study

Pagoda	Plan	Studied eaves	Mean-width observations	Use in analysis
Chaoyang North Pagoda (CY)	Square	E1–E13	13	Main comparison
Chongshou Temple Pagoda (CS)	Octagonal	E1–E13	13	Main comparison
Qingzhou White Pagoda (QZ)	Octagonal	E1–E7	7	Main comparison
Chongxing Temple West Pagoda (CX)	Octagonal	E1–E13	13	Main comparison
Liaoyang White Pagoda (LY)	Octagonal	E1–E13	12	Conditional analysis

Eaves are numbered upward. Relative height runs from the first to the last studied eave, not from the base to the top of the entire tower. Each mean-width observation averages accepted widths along two perpendicular local directions. The four main cases provide 46 observations. Liaoyang provides 12 conditional observations within E1–E13; E9 has no accepted two-direction mean. Case-specific bands, coordinates and model identities are reported in Tables S1–S3 and S12.

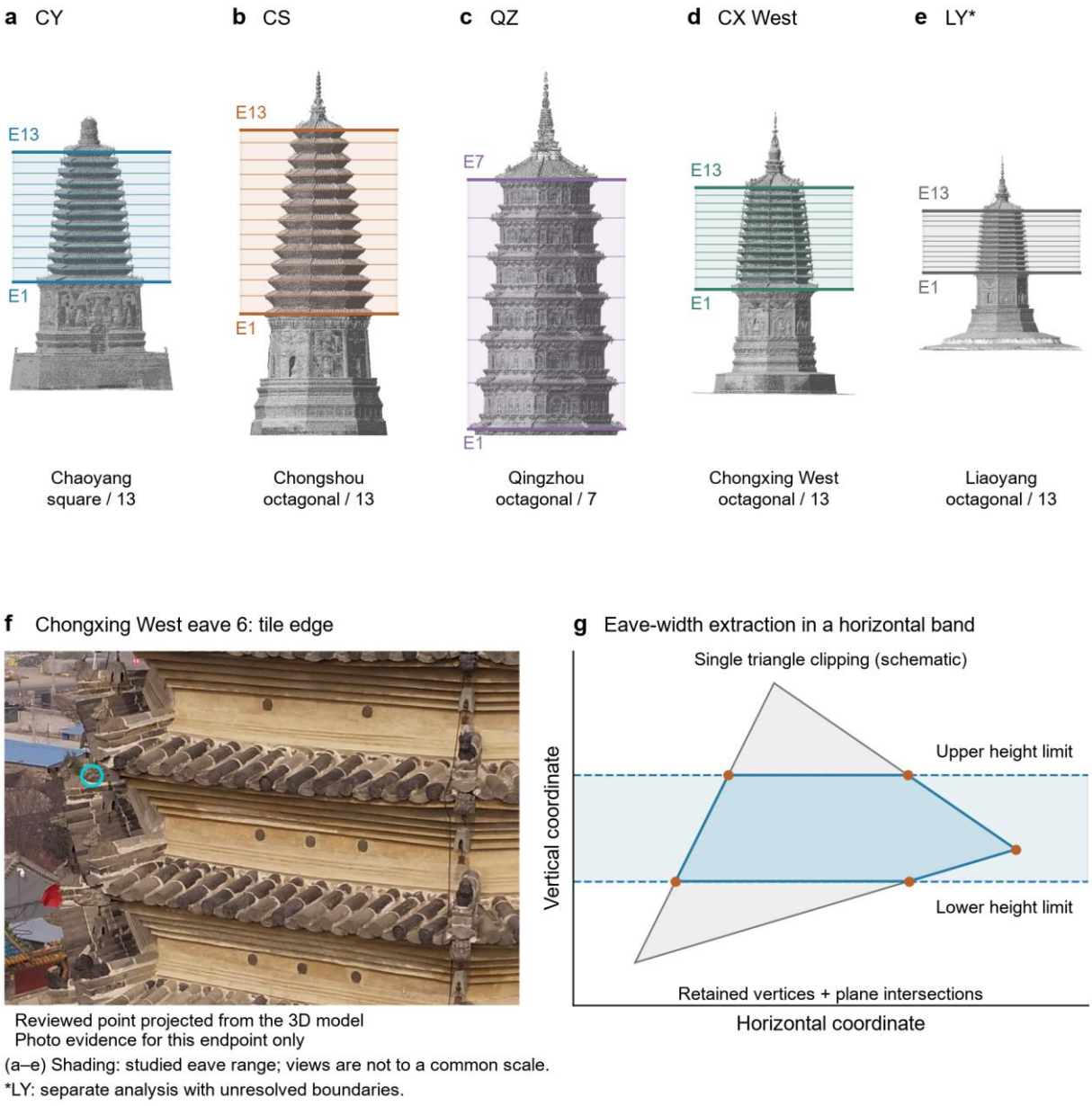


Figure 1 Study ranges and eave-width extraction. (a–e) Source-model views show Chaoyang North (CY), Chongshou Temple (CS), Qingzhou White (QZ), Chongxing Temple West (CX West) and Liaoyang White (LY) Pagodas. E denotes an eave, numbered upward; the numbers below each view give the studied eave counts. Shading spans the first to last studied eaves; horizontal lines locate measurement bands. Views have no common physical scale, and the Qingzhou model is cropped. Liaoyang is analyzed separately with unresolved boundaries and no accepted eave 9 mean width. (f) An original-image crop shows a reviewed tile-edge endpoint at Chongxing West eave 6, projected using ContextCapture camera geometry. (g) A single-triangle schematic illustrates clipping between two horizontal height limits. Blue shading within the triangle marks the retained portion; orange points are retained vertices and edge–plane intersections. This operation is applied to all mesh triangles intersecting the band. The maximum minus minimum X′ and Y′ coordinates of the retained geometry give candidate directional widths; their endpoints then undergo architectural boundary review. The schematic is not a measured pagoda section.

The measurement target is the visible, continuous outer boundary of a specified eave. Review records distinguish tile terminals, masonry projections and the overall eave outline. Bells, chains, vegetation, ornaments and reconstruction artefacts are excluded. Figure 2 connects geometry extraction, boundary review and morphological comparison.

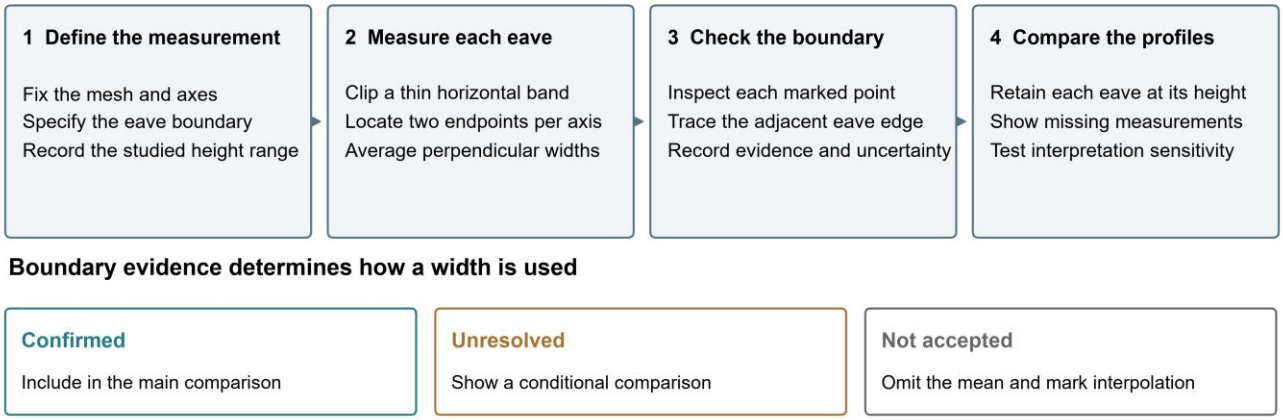


Figure 2 Linking model measurements to architectural comparison. The workflow fixes the measurement target, extracts widths, checks the selected boundaries and compares profiles at their original relative heights. A confirmed boundary can support the main comparison. An unresolved boundary permits only conditional use, while an unaccepted direction leaves the mean width missing. Each decision is retained with the measurement record. Profile widths are divided by the same tower's first studied mean eave width; relative height runs from the first studied eave (0) to the last (1). Conditional use denotes a separate comparison with unresolved boundary evidence.

Width extraction and relative height

The mesh version, mask excluding surrounding geometry, eave selection and coordinate transformation were fixed before width extraction. Z is the vertical axis; X′ and Y′ are perpendicular local analysis directions, rather than shared geographic bearings. Coordinates and widths are expressed in model units. Each source height range was divided into 400 horizontal bands. The QZ crop retained its original grid and band thickness. Tables S1–S3 and S12 specify the transformations, band limits, endpoint coordinates and model identities.

Triangles were clipped against the upper and lower planes of each selected horizontal band. Vertices inside the band and triangle-edge intersections with its planes defined the minimum and maximum coordinates along X′ and Y′ (Fig. 1g). Each directional width is the difference between the maximum and minimum coordinates along that direction. It is not the three-dimensional distance between endpoints, which may differ in height within the band. Equation (1) averages the two widths and normalizes the mean by its first-eave value. Relative height uses the band-center height z_i, with the first and last selected centers defining h = 0 and h = 1.

$$W_i = \frac{W_{x,i} + W_{y,i}}{2}, \quad w_i = \frac{W_i}{W_1}, \quad h_i = \frac{z_i - z_1}{z_n - z_1} \quad (1)$$

Normalized widths refer to the first studied eave, while relative heights refer only to the selected roof sequence. The source model units have not been independently calibrated against physical eave dimensions. Tables S1 and S2 report the eave observations and endpoint coordinates.

Profile comparison

Piecewise-linear interpolation joins retained mean widths at their original relative heights to form $w_t(h)$. Widths at quarter, half and three-quarter height are interpolated and need not coincide with a measured eave. The residual profile $r_t(h)$ subtracts the straight line joining the first and last normalized widths. Its signed area summarizes departures from this reference; positive and negative departures can cancel (Eq. (2)).

$$c_t(h) = 1 + (w_t(1) - 1)h, \quad r_t(h) = w_t(h) - c_t(h) \quad (2a)$$

$$A_t = \int_0^1 r_t(h)\, dh \quad (2b)$$

Relative heights were retained rather than aligning intermediate curve features, preserving differences in where narrowing occurs[14]. Standard L_1, L_2 and maximum distances compare both the original and residual profiles[15].

The L_1 distance integrates the absolute difference; L_2 takes the square root of the integrated squared difference. The maximum distance is the largest absolute separation between profiles. Equation (3) denotes these distances by D_1, D_2 and D_∞, respectively.

$$D_1 = \int_0^1 |w_a(h) - w_b(h)|\, dh \quad (3a)$$

$$D_2 = \sqrt{\int_0^1 (w_a(h) - w_b(h))^2\, dh} \quad (3b)$$

$$D_\infty = max_{0 \le h \le 1} |w_a(h) - w_b(h)| \quad (3c)$$

Distances were calculated on the sorted union of both profiles' relative-height positions. On each interval of length Δh, let u and v denote the profile differences at its two endpoints. The integral of the squared difference is $\frac{\Delta h(u^2 + uv + v^2)}{3}$. When u and v have the same sign or either is zero, the absolute-difference integral is $\frac{\Delta h(|u| + |v|)}{2}$. When their signs differ, the interval is split at the zero crossing and the two triangular areas are added. D_1 sums the absolute integrals; D_2 is the square root of the summed squared integrals. D_∞ is the greatest absolute difference at the combined positions. The same rules apply to the chord-residual profiles.

Boundary review and missing measurements

Review assessed each endpoint's component identity, neighboring continuity, eave tier and boundary definition. Grade A identifies a confirmed architectural boundary; grade B records an unresolved boundary identification; grade C denotes inferred geometry. The records distinguish author confirmations, researcher mesh reviews and inherited judgments. An earlier judgment was retained only when it referred to the same coordinates, frame, target boundary, mask and measurement band. These provenance categories do not represent new independent assessments of every direction.

A mean width requires two retained directional widths. A B-grade direction restricts that mean to the conditional analysis. B records retain local interpretations of the eave outline alongside unresolved component or photograph-to-model correspondence (Table S11). Their retention follows documented assessments of individual locations, rather than a numerical quality threshold.

At LY eave 9, the evidence did not sufficiently establish the intended boundary at the raw X′ endpoints; the targeted follow-up remained unclear. X′ was therefore excluded, while Y′ was retained separately. The historical mirror estimate cannot replace the missing observation. The conditional profile has no two-direction mean at eave 9 and interpolates directly between eaves 8 and 10. Figure 3 shows the photographic and model context for distinguishing eave edges from vegetation and reconstruction gaps.

A separate review exercise presented 12 selected directional widths in a shuffled order, with their earlier grades and values hidden. Reviewers could answer yes, no or unclear. Responses were recorded separately and did not automatically resolve conflicting evidence. Supplementary Note 2 and Tables S10–S11 document the later confirmation of CY eave 2 and the unresolved photograph-marker conflict at LY eave 10.

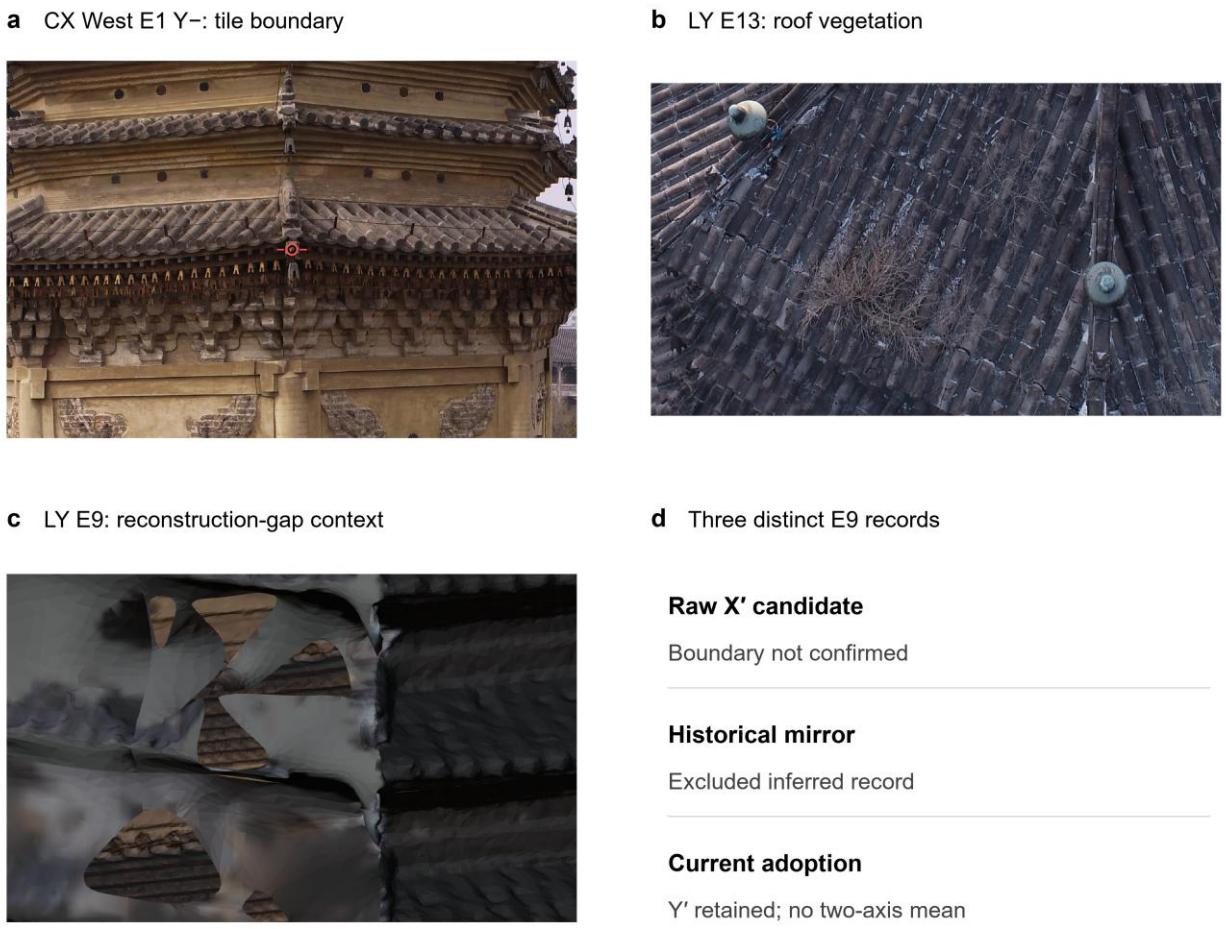


Figure 3 Evidence used to interpret eave boundaries. (a) An archived original-photograph crop of Chongxing West eave 1 Y′− with its existing red projected-coordinate marker. (b) Vegetation at Liaoyang eave 13 is excluded from the measured boundary. (c) The textured model shows a gap at Liaoyang eave 9; the gap alone does not establish that either candidate endpoint is wrong. (d) The raw X′ width, historical mirror estimate and retained Y′ width are separate records. No accepted mean combines them. Image crops retain their original aspect ratios without enhancement or surface repair. CX West and LY denote Chongxing Temple West and Liaoyang White; E indicates the eave number. X′ and Y′ are perpendicular local horizontal axes, and − identifies the negative endpoint. Raw means before boundary review; current adoption means the measurements retained after review.

Sensitivity to measurement choices

Each of 48 internal mean-width observations was omitted in turn, retaining the original height limits and first-width denominator. The targeted CY eave 2 test joins eaves 1 and 3 directly. Separate tests shifted all selected measurement bands in a case by −2, −1, 0, +1 or +2 band indices. Relative heights remained fixed, while the shifted first-band width supplied the denominator (Eq. (4)). The five offsets per case pair yield 25 combinations per case pair. LY eave 9 remains missing.

$$w_i^{(\delta)}(h_\mathrm{i}) = \frac{W_i^{(\delta)}}{W_1^{(\delta)}}, \quad h_\mathrm{i}\, fixed, \quad \delta \in \{-2,-1,0,1,2\} \quad (4)$$

Additional tests isolated normalization by replacing only the first-width reference with a neighboring-band width. Other widths and original heights were retained, and w(0) was restored to 1. Thickness tests used half, original and double band thickness at unchanged centers, each normalized by its own first width. We tracked the signed quarter-height difference and complete-profile distances. These are specified numerical scenarios rather than confidence intervals.

Uniform surface sampling of the fixed CX mesh used Open3D to draw 150,000 or 500,000 points per realization. Before each draw, its random generator was set to one of the ten seeds 1101–1110. Points were assigned by height to the frozen 400-band grid. Bands included their lower boundary and excluded their upper boundary, except that the highest point was assigned to the final band. The selected eave bands were fixed; no new peak search was performed. Each evaluated band required at least ten sampled points. Width loss compares a sampled width with the full-mesh width in the same band (Eq. (5)). Neighboring-band tests used offsets up to ±2; local direction tests used rotations of −1°, −0.5°, 0°, +0.5° and +1°. These tests sample the existing mesh rather than independently survey the building.

$$L = 100\,(1 - \frac{W_{sample}}{W_{mesh}})\% \quad (5)$$

Horizontal directions were tested from 0° to 89° at 1° intervals. Each tested direction was held constant across all eaves of a pagoda. Directions were varied independently between pagodas. Widths came from planar convex hulls of triangles clipped to each measurement band. Equation (6) defines the mean width along two perpendicular directions $M_i(\theta)$, area-equivalent diameter d_i and Cauchy mean width b_i. The latter two use hull area S_i and perimeter P_i. Each width definition used its own first-eave denominator and the original relative heights.

$$M_i(\theta) = \frac{W_i(\theta) + W_i(\theta + 90°)}{2} \quad (6a)$$

$$d_i = 2\sqrt{\frac{S_i}{\pi}}, \quad b_i = \frac{P_i}{\pi} \quad (6b)$$

Convex hulls bridge gaps and retain attached geometry. Their widths test sensitivity to geometric representation; they have not received the same architectural boundary review as the adopted measurements. Extrema from shifted or thicker bands were also treated as diagnostic values, rather than newly confirmed boundaries.

Comparison before and after boundary review

The calculation before boundary review is termed raw: it used the geometric width candidates. The calculation after review is termed adopted: it retained only measurements allowed by the documented boundary decisions. Both used identical meshes, masks, transformations, eave selections, bands, axes and normalization. We compared widths retained in both calculations and assessed the effect of excluding the unconfirmed mean at LY eave 9. The historical mirror estimate was assessed separately. Buildings were the descriptive units; eaves, sampling seeds and numerical scenarios were not independent buildings.

Four Python programs reproduced profile comparisons and diagnostics from unchanged exported observations. The recorded replay environment used Python 3.12.14, NumPy 2.3.5 and pandas 3.0.1. The original surface-sampling environment used Python 3.12.14, Open3D 0.19.0, NumPy 2.5.3 and pandas 3.0.5. These were separate environments. Input checksums verified that replay did not alter the input tables. Recalculation from exported observations checks numerical consistency; it does not repeat geometry extraction or independently establish agreement with physical dimensions.

Results

Chaoyang narrowed earlier than Chongshou despite similar total width reductions

Chaoyang North (CY) and Chongshou Temple (CS) reached almost the same last-to-first studied eave-width ratios, 0.4841 and 0.4892, through different patterns of narrowing (Table 2; Fig. 4). Between the first two eaves, CY lost 19.93% of its first-eave width, compared with 0.63% in CS. The second eaves occupied similar relative

heights, 0.1058 and 0.0990. The larger early reduction in CY therefore occurred over a comparable part of the studied height range.

This contrast extended beyond the first transition. At one-quarter of the height between the first and last studied eaves, CY retained 75.92% of its own first-eave width and CS retained 89.76%. This interpolated position lay between the third and fourth eaves in both cases. Their normalized widths became closer farther up the sequences: 0.7000 and 0.7610 at half height, and 0.6274 and 0.6340 at three-quarter height. CY had thus undergone more of its width reduction in the lower sequence, while CS narrowed later to reach a similar final proportion.

Comparison with a straight line between the first and last widths showed the same distinction. CY lay below this reference over the lower sequence, while CS lay above it over much of the lower and middle sequence. Their signed residual areas were −0.0451 and +0.0185. The integrated absolute difference between their profiles, D_1, was 0.0674 and changed little after subtracting the endpoint reference, to 0.0663. The profile difference therefore arose mainly from where narrowing occurred, rather than from their similar last-to-first width ratios.

Qingzhou showed less initial narrowing across a larger relative height interval

Qingzhou White (QZ) and Chongxing Temple West (CX) differed in the combination of eave spacing and width reduction (Table 2; Fig. 4). Between the first two studied eaves, QZ lost 7.14% of its first-eave width over 0.1822 of the studied height range. CX lost 11.16% over a shorter relative-height interval of 0.1119. The first transition in QZ therefore combined greater relative spacing with a smaller proportional width reduction.

QZ also retained a larger fraction of its first-eave width farther up the sequence. At quarter height, the normalized widths were 0.9113 for QZ and 0.8671 for CX; the corresponding values were 0.8352 and 0.8037 at half height, and 0.7591 and 0.7376 at three-quarter height. Their last-to-first ratios were relatively close, at 0.6857 and 0.6697. Quarter height fell between QZ eaves 2 and 3 but between CX eaves 3 and 4, reflecting their seven- and thirteen-eave organizations (Fig. 1c,d). Comparing relative heights revealed the width difference without equating tiers that occupied different positions in the studied sequences.

Table 2 Width retention and narrowing within the studied eave sequences

Case	Last/first width	First-to-second change	Width at quarter height	Signed departure area
CY	0.4841	−19.93%	0.7592	−0.0451
CS	0.4892	−0.63%	0.8976	+0.0185
QZ	0.6857	−7.14%	0.9113	−0.0059
CX	0.6697	−11.16%	0.8671	−0.0295
LY*	0.7474	−8.15%	0.8847	−0.0310

Widths are normalized by the mean width of the first studied eave. Quarter height is h = 0.25 within the first-to-last study range; the listed widths are interpolated profile values. Signed departure area is the integral of the normalized profile minus its first-to-last straight-line reference. Positive and negative departures can cancel. * LY is conditional. Its E9 mean is missing, and the line between E8 and E10 is interpolation rather than a measured E9 value.

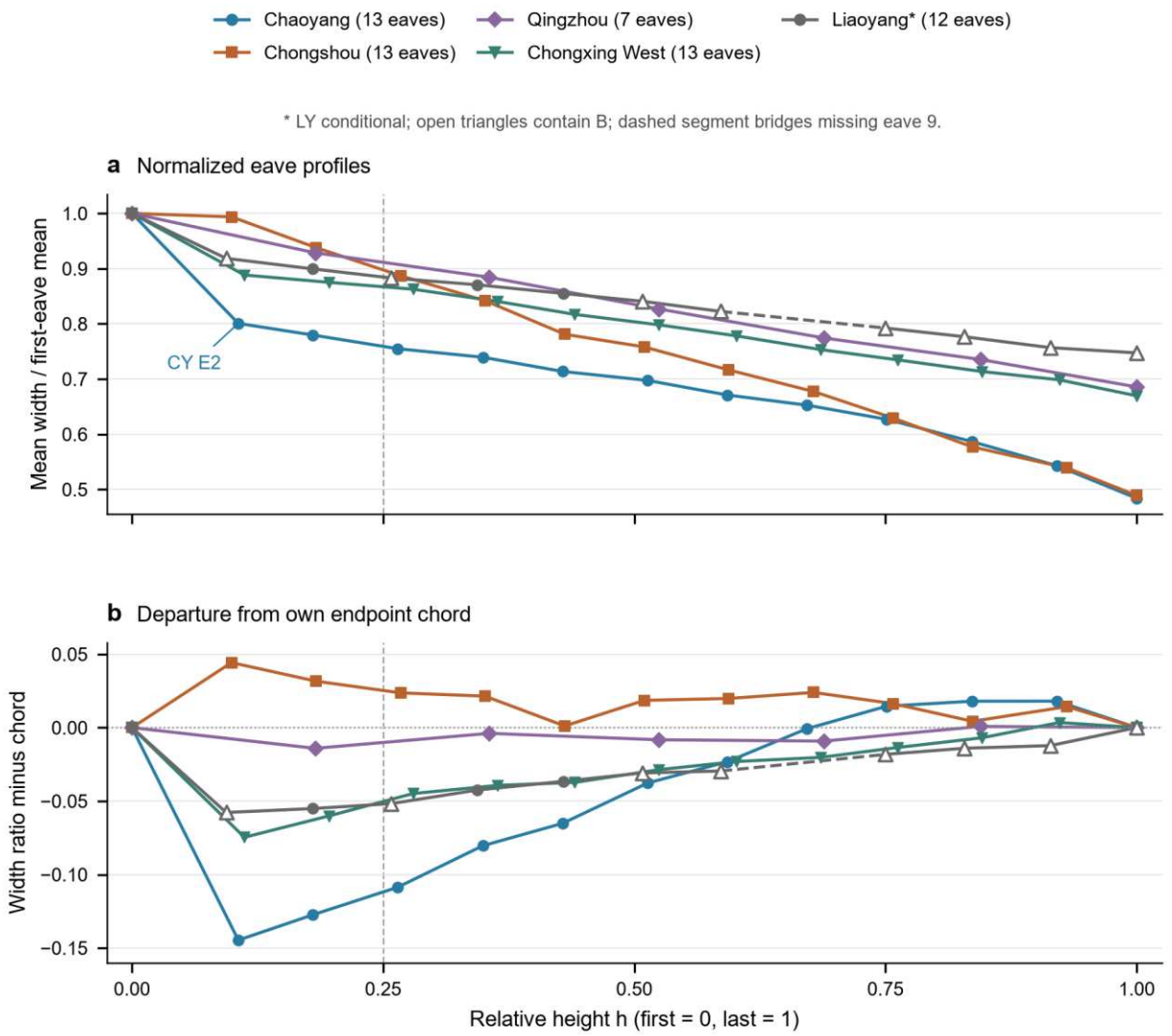


Figure 4 Width profiles locate differences along the studied roof sequences. (a) Each mean eave width is divided by the same tower's first studied mean width. Relative height h runs from the first studied eave (0) to the last (1), excluding the rest of the tower. CY E2 identifies Chaoyang North eave 2; the vertical dashed line marks quarter height. (b) Residual profiles subtract the straight line joining each profile's first and last values (the endpoint chord). The four main cases contribute 46 mean-width observations. Liaoyang (LY) contributes 12; its asterisk denotes separate conditional analysis. Open triangles mark means containing at least one unresolved boundary (grade B). Its dashed eave 8–10 segment interpolates across the missing eave 9 mean. All plotted widths and residuals are dimensionless.

The quarter-height contrasts persisted under alternative measurement choices

The quarter-height contrasts were tested to distinguish differences that persisted from those that depended on measurement choices. CY retained a smaller fraction of its first-eave width than CS in both omission and band-shift tests (Table 3; Fig. S1). The 22 omission scenarios gave D_1 values of 0.0611–0.0689, compared with 0.0674 in the adopted calculation; 25 band-shift combinations gave 0.0544–0.0710. Omitting CY eave 2 reduced D_1 by 9.30% (Fig. 5), but changed the interpolated profile only below eave 3, at relative height 0.1799. The quarter-height contrast therefore did not depend on eave 2. Locating the early reduction specifically between eaves 1 and 2 did depend on that observation.

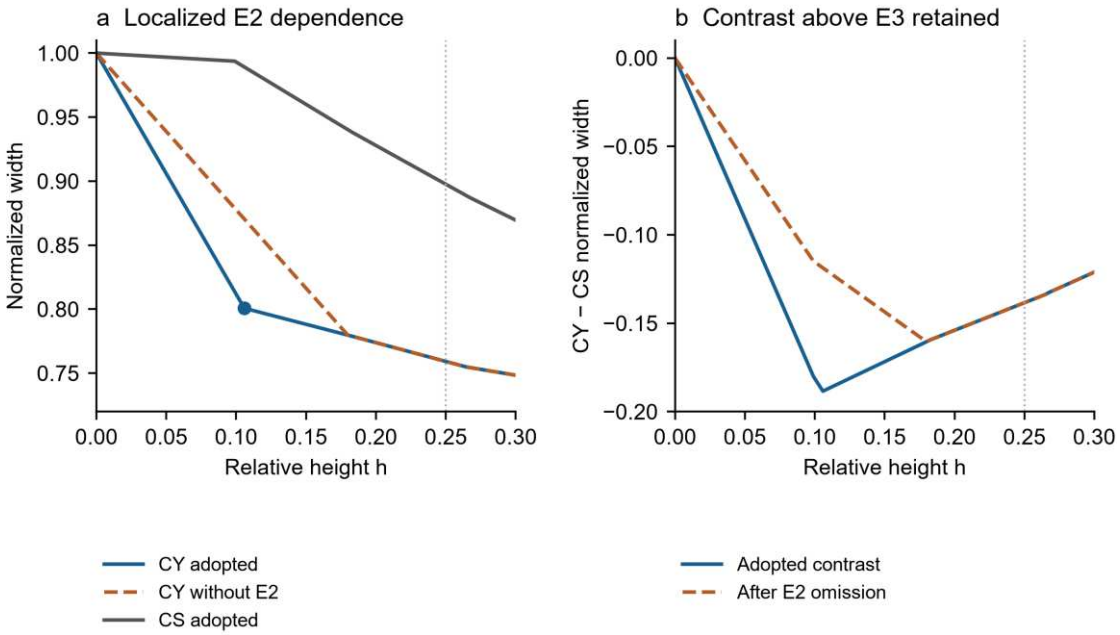


Figure 5 Effect of omitting Chaoyang North eave 2. CY and CS denote Chaoyang North and Chongshou Temple; E denotes the eave number. (a) Width profiles near the lower eaves, with CY recalculated after eave 2 is omitted. Adopted denotes the measurements retained after boundary review. (b) CY minus CS normalized widths before and after omission. Each width is divided by its tower's first studied mean width; h = 0 and 1 locate the first and last studied eaves. These references remain fixed after omission. D_1, the integrated absolute difference between profiles, decreases by 9.30%. The CY profiles coincide from eave 3 (h = 0.1799) upward, leaving the quarter-height contrast unchanged. The dotted line marks h = 0.25.

QZ retained a larger relative width than CX at quarter height in all 16 omission scenarios and all 25 band-shift combinations. However, the size of the profile difference was sensitive to measurement choices. Band shifts changed D_1 to 0.0164–0.0382, or −48.1% to +20.8% relative to the adopted value. Changing only the first-width reference widened the range to 0.0105–0.0546, or −66.8% to +72.9%. The relative-width ordering at quarter height was also unchanged in all nine combinations of band thickness for each pair. These outcomes support the relative-width ordering at that height more consistently than a particular distance magnitude or exact transition location.

The quarter-height contrasts also persisted when the horizontal measurement directions were varied independently between cases. Across the tested direction pairs, CY–CS D_1 ranged from 0.0623 to 0.0725, while QZ–CX ranged from 0.0201 to 0.0326 (Fig. 6). Area-equivalent widths gave corresponding distances of 0.0671 and 0.0242. The area-equivalent profile distance for QZ–CX was 23.3% below the distance based on the adopted widths. Alternative width definitions therefore preserved the relative-width ordering at quarter height, while changing the distances between the complete profiles. Their convex boundaries were used for this diagnostic comparison and were not treated as newly confirmed architectural edges.

Table 3 Sensitivity of the two principal morphological contrasts

Pair	Measurement change	n	Profile distance D_1	Quarter-height difference
CY–CS	Omit one internal eave	22	0.0611 to 0.0689	−0.1407 to −0.1345
CY–CS	Shift all measurement bands	25	0.0544 to 0.0710	−0.1421 to −0.1144
CY–CS	Change first-width reference	25	0.0641 to 0.0787	−0.1542 to −0.1331
CY–CS	Change band thickness	9	0.0658 to 0.0681	−0.1393 to −0.1350
QZ–CX	Omit one internal eave	16	0.0277 to 0.0338	0.0414 to 0.0516
QZ–CX	Shift all measurement bands	25	0.0164 to 0.0382	0.0290 to 0.0546
QZ–CX	Change first-width reference	25	0.0105 to 0.0546	0.0140 to 0.0724
QZ–CX	Change band thickness	9	0.0273 to 0.0327	0.0407 to 0.0453

n is the number of numerical scenarios. D_1 is the integrated absolute difference between the normalized profiles. The baseline values are 0.0674 for CY–CS and 0.0316 for QZ–CX. Ranges are minima and maxima over specified numerical scenarios, not confidence intervals. Quarter-height differences are the first case minus the second; every listed scenario retains the baseline sign. Omission removes one internal mean-width observation. Band shifts retain the original relative heights; first-width tests change only the denominator. Thickness tests use half, original and double thickness. The number of scenarios is not a count of independent buildings or reviewers. Complete results, including direction and alternative-width tests, are reported in Tables S5, S7 and S8.

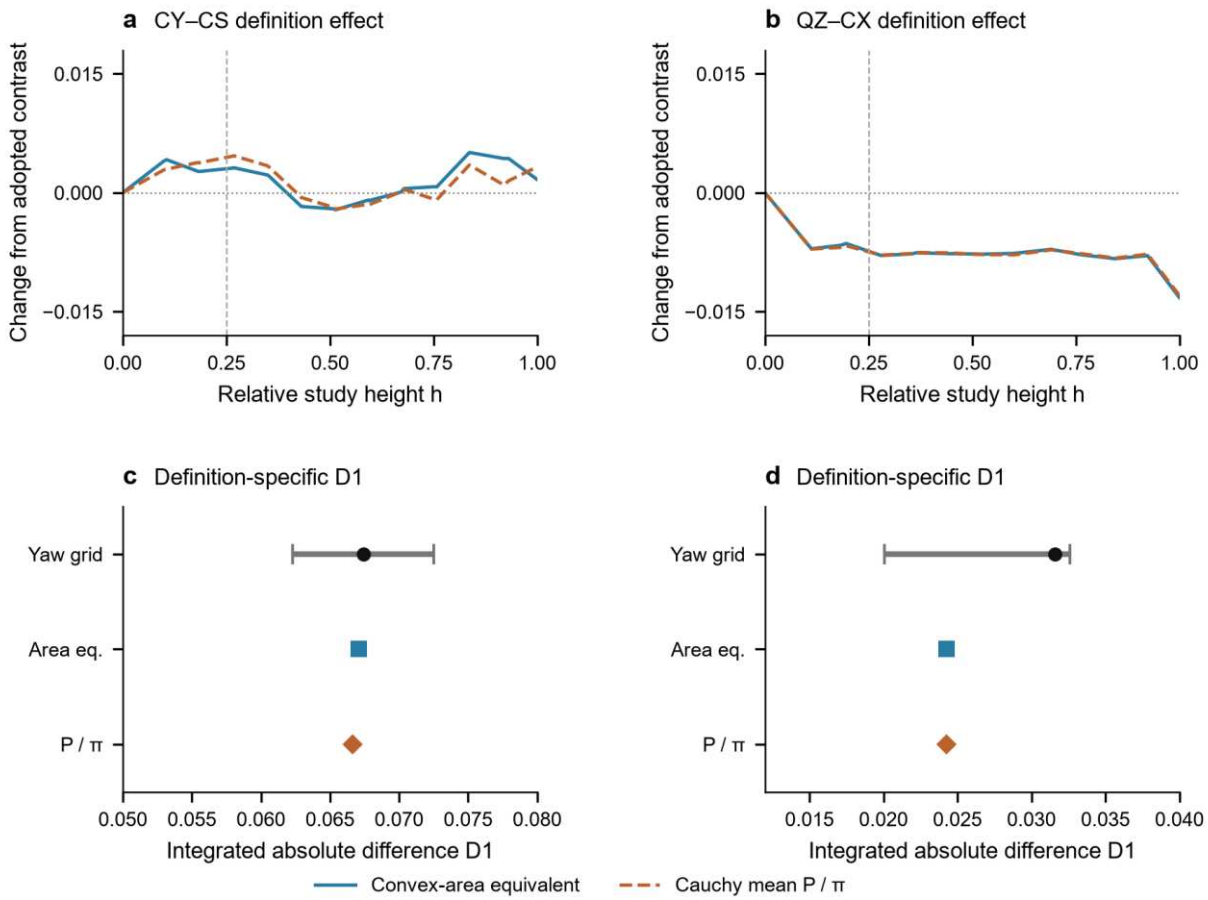


Figure 6 Sensitivity to horizontal direction and width definition. CY, CS, QZ and CX denote Chaoyang North, Chongshou Temple, Qingzhou White and Chongxing Temple West. (a,b) Changes in the between-tower contrast when alternative widths replace the two-direction means retained after review (adopted). Each contrast is the first tower's normalized width minus the second's; the plotted change subtracts the adopted contrast. Blue solid lines use area-equivalent width; orange dashed lines use Cauchy mean width, the convex-hull perimeter P divided by π. Each definition uses its own tower-specific first-eave denominator. Relative height h spans the first (0) to last (1) studied eaves; the vertical dashed line marks h = 0.25. (c,d) D_1 is the integrated absolute difference between normalized profiles. Yaw grid bars span 8,100 horizontal-direction combinations, not confidence intervals. Circles show adopted D_1, squares area-equivalent D_1 and diamonds Cauchy-mean D_1. Convex-hull widths are diagnostic alternatives without new architectural boundary review.

Sampling the fixed CX mesh more densely reduced missed width: median loss fell from 1.10% to 0.52% and maximum loss from 3.03% to 1.71% between 150,000 and 500,000 surface points. This supports checking geometric extraction independently of architectural interpretation, but does not test agreement with a building survey. Full direction, omission, band and sampling results are in Tables S5–S9.

An uncertain Liaoyang edge affected local interpretation more than profile distances

Boundary review left the contrasts among the four main cases unchanged. The 117 retained directional widths and 58 two-direction mean widths common to the calculations before and after review had identical values. The consequential change was the exclusion of Liaoyang eave 9 X′: its unconfirmed boundary prevented a two-direction mean from being used at that height. The counts and remaining unresolved directions are documented in Tables 1 and S11.

The Liaoyang profile consequently connects eaves 8 and 10 without a measured mean at eave 9 (Fig. 7). The resulting segment describes interpolation across the gap, rather than the shape of that individual roof. Table 4

shows why this case is treated differently from a confirmed Chongxing West boundary and a Liaoyang boundary retained for conditional analysis.

Excluding the LY eave 9 mean changed the normalized profile locally by at most 0.0047. Each of the four integrated absolute profile differences, D_1, involving LY decreased by 3.84×10^{-4}, equivalent to reductions of 0.26–1.44%, without changing their ordering. These four changes followed from the same omission and were not independent tests. Review therefore changed the evidence available for the Liaoyang comparison, with a small effect on these profile distances, rather than correcting the retained widths.

A second review did not resolve all uncertainty: the new heritage-trained reviewer marked Liaoyang eave 9 X′ as unclear and confirmed the marked model edge at eave 10 X′. The latter remained conditional because that interpretation did not resolve the earlier photograph-marker conflict. These responses qualify the earlier reviewer's affirmative answers and are retained separately in Tables S10–S11.

Table 4 How boundary evidence determines the use of three measurements

Measurement	Raw width	Width used	Boundary assessment	Use in analysis
CX West E6 X′	10.6774	10.6774	Confirmed boundary (A)	Included in the main comparison
LY E13 X′	14.9978	14.9978	Boundary still unresolved (B)	Used only in the LY conditional profile
LY E9 X′	16.3250	—	Not accepted	No mean width for LY E9; raw diagnostic only

Widths are in local model units. A denotes component-based boundary confirmation, not independent confirmation of physical dimensions. B retains an unresolved boundary identification. All 117 retained directional widths are numerically unchanged. The audit changes which measurements support a comparison, rather than correcting those retained widths. LY E9 X′ is an unaccepted raw geometric measurement. The historical mirrored X′ estimate is a different record and is also excluded; the accepted Y′ width is retained separately and cannot replace the missing X′ measurement. The 15 unresolved LY directions remain B. The R12 follow-up concerns LY E10 X′, not E13 X′; its affirmative model interpretation did not resolve the earlier photograph-marker conflict.

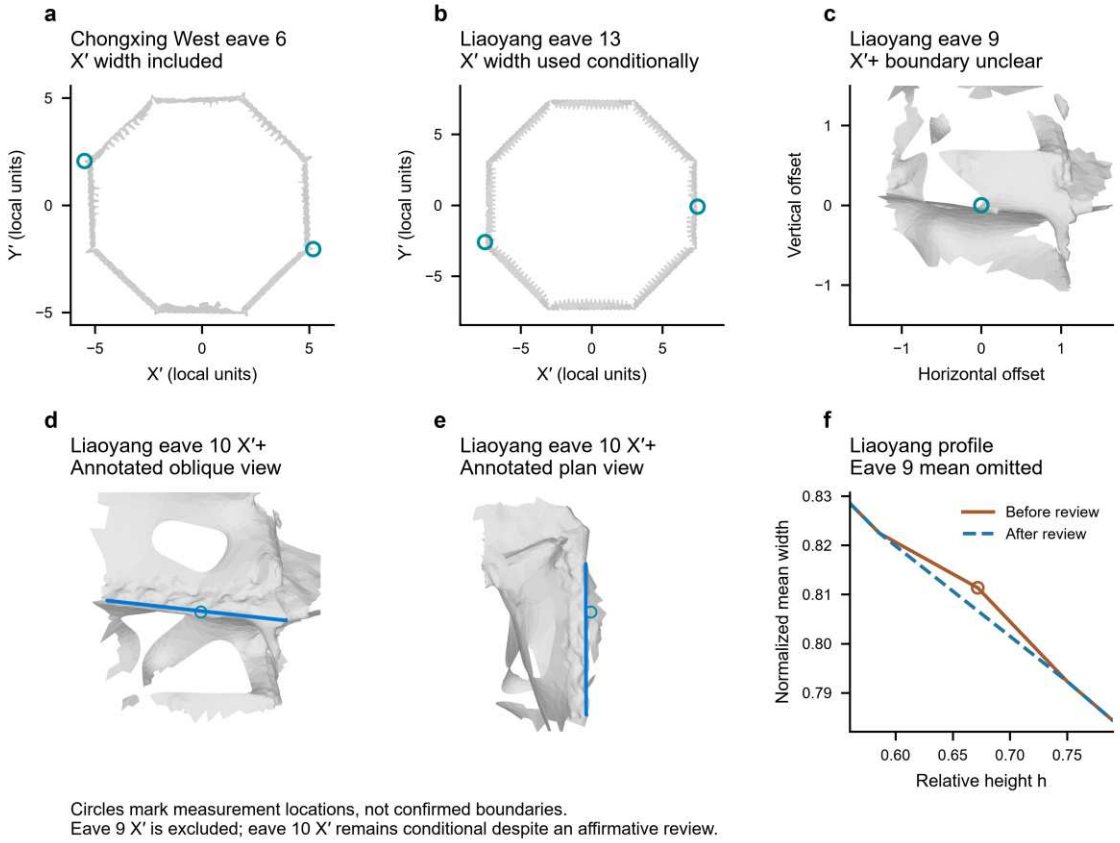


Figure 7 Boundary evidence determines measurement use. (a,b) Plan views locate the recorded X′ endpoints at Chongxing West eave 6 and Liaoyang eave 13. The former supports the main comparison; the latter remains conditional. (c) R07 shows Liaoyang eave 9 X′+ in the original untextured mesh. R2 answered unclear; this direction remains excluded following boundary review. (d,e) Crops from the author-supplied revised R12 plate show straight blue boundary annotations at Liaoyang eave 10 X′+. R2 answered yes and retained the point. Its measurement remains conditional because the earlier original-image conflict is unresolved. (f) Excluding the eave 9 mean changes the interpolation between eaves 8 and 10. Circles locate coordinates rather than certify boundaries. Offsets are model units, and cropped views have no common physical scale. R07 and R12 are review-item identifiers, and R2 is the second reviewer. In (f), mean width is divided by Liaoyang's first studied mean width; relative height spans its first (0) to last (1) studied eaves. Before review includes the raw eave 9 mean; after review omits it. Neither curve uses the historical mirror estimate.

Table S4 reports the four affected LY comparisons. Tables S10 and S11 retain the human responses and the unresolved directions, including affirmative responses that did not settle an existing evidence conflict.

Discussion

The comparisons distinguish two architectural aspects of narrowing: where width reduction is concentrated, and how that reduction relates to the spacing of roofs. Chaoyang and Chongshou illustrate the first. Their similar final width proportions conceal a pronounced difference in the lower sequence that becomes much smaller higher up. Qingzhou and Chongxing West illustrate the second: a longer lower roof interval can accompany less proportional narrowing. Describing these differences by location makes the outline useful for selecting architectural observations, rather than treating a single measure of total taper as a sufficient description of the building.

For Chaoyang and Chongshou, the lower roof assemblies are the priority for explaining the contrast. The second eaves lie at similar relative heights, so the early difference is not an artefact of matching tier numbers at different

positions. The convergence of the normalized widths farther up the sequence also directs attention downward. This does not establish that Chaoyang is physically narrower: each value expresses the width retained relative to that tower's own first studied eave. Instead, it shows that the relation between the lower roofs and the first roof differs substantially between the two buildings.

Published descriptions identify components that could be examined at this location. Chaoyang is described as a square, hollow brick pagoda with thirteen corbelled eaves and a layered construction and repair history[16]. At Chongshou, the first roof assembly includes brackets, timber rafters and tiled roofing; above it, a very low wall precedes upper corbelled eaves described as closely adjoining without intervening wall surfaces[17]. This distinction matters for interpreting the width profile. The first roof cannot automatically be treated as a repeated version of every roof above it, and an exposed wall band should not be assumed between all Chongshou eaves. These descriptions support examining the transition between assemblies, but supply no dimensions that would establish its contribution to the measured narrowing.

The profile therefore identifies an unresolved component question at a specific location (Fig. 1a,b): does the early contraction mainly reflect the reach of the first roof, a change in the supporting body, or both? Corresponding sections through the first few roofs could separate wall-face position, bracket or corbel projection, and the terminal roof edge. Their offsets would distinguish a change in roof projection from a change in body width. This is a more focused investigation than remeasuring the overall taper. The visible geometry and published descriptions identify what to compare; assigning the contrast to a repair episode would additionally require dated construction evidence.

For Qingzhou and Chongxing West, the important unit is the interval between roofs. Less initial narrowing over a longer relative-height interval means that Qingzhou retains more of its first-eave width across a greater fraction of the studied height. Its greater width retention at quarter height is consistent with this lower-sequence organization. Matching only eave numbers would obscure the distinction, because quarter height falls in different roof intervals. The comparison instead relates horizontal reduction to vertical position while leaving floor and tier identities specific to each building.

The component descriptions and context views help locate this difference without explaining its cause. Qingzhou's seven-tier arrangement includes timber rafters above brick brackets[18], and Waugh's photographic account identifies bracket forms rendered in brick[19]. The official account of the Chongxing twins describes thirteen eaves, with brick brackets below the first roof and corbelled projections above[20]; the model owner identifies the analyzed tower as the west tower. The readily distinguishable intervening body surfaces at Qingzhou and the more closely stacked roof sequence at Chongxing West are visible in Fig. 1c,d. These observations provide an architectural context for the measured spacing contrast. The views are not at a common physical scale, and the interval between measured edges includes roof components as well as any exposed wall.

A useful follow-up would therefore separate the height occupied by each lower roof assembly from the visible body between roofs, then measure the lateral offsets from body to roof edge. That comparison could establish whether Qingzhou's more gradual initial narrowing is associated chiefly with body geometry, roof projection or their combination. The present profiles identify the intervals in which this distinction matters. They do not show that seven-tier pagodas generally narrow differently from thirteen-eave pagodas, or that timber and brick account for the contrast: tier count, material and structural arrangement vary together in this pair.

The contribution to architectural comparison is the connection between a difference in overall form and the roof locations at which it can be investigated. Proportional and parametric studies address dimensional relationships[1,2], while axis and symmetry studies characterize alignment and regularity[5,6]. The present evidence adds the distribution of width reduction along a selected sequence. Normalization and interpolation provide the

means of comparison; their usefulness is demonstrated here by the architectural distinctions they reveal. The framework makes those distinctions traceable to particular edges and their evidence, so that a reader can distinguish a recorded roof from an inferred segment of the profile.

The reliability results support some interpretations more strongly than others. Both quarter-height contrasts persist under the tested choices, supporting the location of the differences in the lower sequences. Distances and the positions of maximum separation vary, so neither should be treated as a fixed architectural property independent of measurement definition. Omitting Chaoyang eave 2 preserves the quarter-height contrast but changes the earlier segment: the general lower-sequence finding is less dependent on that eave than the specific first-transition finding. Convex-width alternatives and shifted bands help expose such dependence; they remain diagnostic comparisons because their new boundaries have not undergone architectural review.

Liaoyang shows why a small numerical change can still matter to architectural interpretation. Omitting eave 9 changes profile distances little, but removes the basis for describing that roof through a two-direction mean. Interpolation can preserve a useful broader comparison without establishing the local boundary. In this respect, the review gives provenance and defect documentation[10,11] a concrete role in morphological interpretation: it identifies where a statement concerns observed geometry and where it crosses an evidential gap. Because retained widths did not change, this example demonstrates a restriction on interpretation rather than improved dimensional accuracy.

The cases describe available buildings and meshes, rather than isolating plan, material, construction period or acquisition history. CY is square in plan and the others are octagonal, and the height range excludes the base, lower body below the first studied eave and finial. Independent measurements of the same boundaries would be required to establish dimensional accuracy[21,22]. Original images, registered projections and RTK records assist interpretation but share acquisition or reconstruction history with the models. The small targeted human-review exercise likewise cannot estimate performance across all endpoints: responses were relayed by the author, and R2's inspected materials were incompletely documented. Residual model tilt and application to additional buildings remain to be tested.

The findings establish a focused use for height-resolved eave profiles: locating differences that an overall reduction ratio conceals and identifying the component observations needed to explain them. For Chaoyang and Chongshou, the next comparison concerns body and roof offsets in the first few assemblies; for Qingzhou and Chongxing West, it concerns the components occupying the lower roof intervals and their projections. The same reasoning can guide a new application once its architectural boundary and supporting evidence have been established. The five cases demonstrate this use, while broader transfer and explanations of construction history require further evidence.

References

1. Wang, S. et al. Morphological Study on Multi-storied Brick Pagodas of the Tang Dynasty: An Analysis Method Based on Historical Patterns and Mathematical Models. Int. J. Archit. Herit. 15, 1655–1670 (2021). https://doi.org/10.1080/15583058.2020.1712497

2. Qiu, G. & Cheng, B. A Study on the Application of Parametric Geometry in the Morphology of Qing Dynasty Multi-Storey Pavilion-Style Pagoda in Northeast Sichuan. Buildings 16, 2749 (2026). https://doi.org/10.3390/buildings16142749

3. Gao, M., Wang, N. & Wang, Z. Constituent Elements of Dense-Eaves Brick Pagodas in the Liao Dynasty [in Chinese]. J. Archit. Hist. 3, 136–153 (2022). https://doi.org/10.12329/20969368.2022.03016

4. Remondino, F. Heritage Recording and 3D Modeling with Photogrammetry and 3D Scanning. Remote Sens. 3, 1104–1138 (2011). https://doi.org/10.3390/rs3061104

5. Chan, T.O. et al. CENTRAL AXIS ESTIMATION FOR ANCIENT CHINESE PAGODAS BASED ON GEOMETRIC MODELLING AND UAV-BASED PHOTOGRAMMETRY. Int. Arch. Photogramm. Remote Sens. Spat. Inf. Sci. XLIII-B2-2020, 751–756 (2020). https://doi.org/10.5194/isprs-archives-xliii-b2-2020-751-2020

6. Chan, T.O. et al. Symmetry Analysis of Oriental Polygonal Pagodas Using 3D Point Clouds for Cultural Heritage. Sensors 21, 1228 (2021). https://doi.org/10.3390/s21041228

7. Moyano, J., Nieto-Julián, J.E., Bienvenido-Huertas, D. & Marín-García, D. Validation of Close-Range Photogrammetry for Architectural and Archaeological Heritage: Analysis of Point Density and 3D Mesh Geometry. Remote Sens. 12, 3571 (2020). https://doi.org/10.3390/rs12213571

8. Marčiš, M., Fraštia, M., Kovanič, Ľ. & Blišťan, P. Deformations of Image Blocks in Photogrammetric Documentation of Cultural Heritage—Case Study: Saint James's Chapel in Bratislava, Slovakia. Appl. Sci. 13, 261 (2023). https://doi.org/10.3390/app13010261

9. Yang, S., Hou, M. & Li, S. Three-Dimensional Point Cloud Semantic Segmentation for Cultural Heritage: A Comprehensive Review. Remote Sens. 15, 548 (2023). https://doi.org/10.3390/rs15030548

10. Guillem, A. et al. Bridging the Provenance Knowledge Gap Between 3D Digitization and Semantic Interpretation. Heritage 8, 476 (2025). https://doi.org/10.3390/heritage8110476

11. Sullini, M. When meshes lie formalising tacit knowledge for flaw recognition in cultural heritage photogrammetry. Digit. Appl. Archaeol. Cult. Herit. 41, e00534 (2026). https://doi.org/10.1016/j.daach.2026.e00534

12. Campos, M., Tommaselli, A., Ivánová, I. & Billen, R. Data Product Specification Proposal for Architectural Heritage Documentation with Photogrammetric Techniques: A Case Study in Brazil. Remote Sens. 7, 13337–13363 (2015). https://doi.org/10.3390/rs71013337

13. Homburg, T., Cramer, A., Raddatz, L. & Mara, H. Metadata schema and ontology for capturing and processing of 3D cultural heritage objects. Herit. Sci. 9, 91 (2021). https://doi.org/10.1186/s40494-021-00561-w

14. Wu, Y., Huang, C. & Srivastava, A. Shape-based functional data analysis. TEST 33, 1–47 (2024). https://doi.org/10.1007/s11749-023-00876-9

15. Ramos-Carreño, C., Torrecilla, J.L., Carbajo-Berrocal, M., Marcos, P. & Suárez, A. scikit-fda : A Python Package for Functional Data Analysis. J. Stat. Softw. 109, 1–37 (2024). https://doi.org/10.18637/jss.v109.i02

16. Liaoning Department of Culture and Tourism. Chaoyang North Pagoda [in Chinese]. Official monument description (27 August 2020). https://whly.ln.gov.cn/whly/wlzt/lnww/zdwwbhdw/8A68EB2D6A244A1F8C64DA4A1DB8E4FC/index.shtml (accessed 13 October 2026).

17. Liaoning Department of Culture and Tourism. Chongshou Temple Pagoda [in Chinese]. Official monument description (27 August 2020). https://whly.ln.gov.cn/whly/wlzt/lnww/zdwwbhdw/A676CB9D1B3B47B5AB99E044B72A7118/index.shtml (accessed 13 October 2026).

18. Bairin Right Banner People's Government. Liao Shakyamuni Relic Pagoda [in Chinese]. Official monument description (26 April 2023). https://www.blyq.gov.cn/zjbl/jqjd/202304/t20230426_2043610.html (accessed 13 October 2026).

19. Waugh, D.C. Light on the Liao: A Photo Essay. Silk Road 15, 83–106 (2017). https://edspace.american.edu/silkroadjournal/wp-content/uploads/sites/984/2018/03/Waugh_Liao_SR_15_2017_pp83_106.pdf

20. Liaoning Department of Culture and Tourism. Twin Pagodas of Chongxing Temple [in Chinese]. Official monument description (27 August 2020). https://whly.ln.gov.cn/whly/wlzt/lnww/zdwwbhdw/C6DB74C77FCD45C2BAA94B7A924CCF78/index.shtml (accessed 13 October 2026).

21. Nocerino, E., Menna, F. & Remondino, F. Accuracy of typical photogrammetric networks in cultural heritage 3D modeling projects. Int. Arch. Photogramm. Remote Sens. Spat. Inf. Sci. XL-5, 465–472 (2014). https://doi.org/10.5194/isprsarchives-xl-5-465-2014

22. De Fino, M., Galantucci, R.A. & Fatiguso, F. Condition Assessment of Heritage Buildings via Photogrammetry: A Scoping Review from the Perspective of Decision Makers. Heritage 6, 7031–7067 (2023). https://doi.org/10.3390/heritage6110367

Supplementary Files

This is a list of supplementary files associated with this preprint. Click to download.

- SupplementaryInformation.pdf